Provided for non-commercial research and education use.
Not for reproduction, distribution or commercial use.

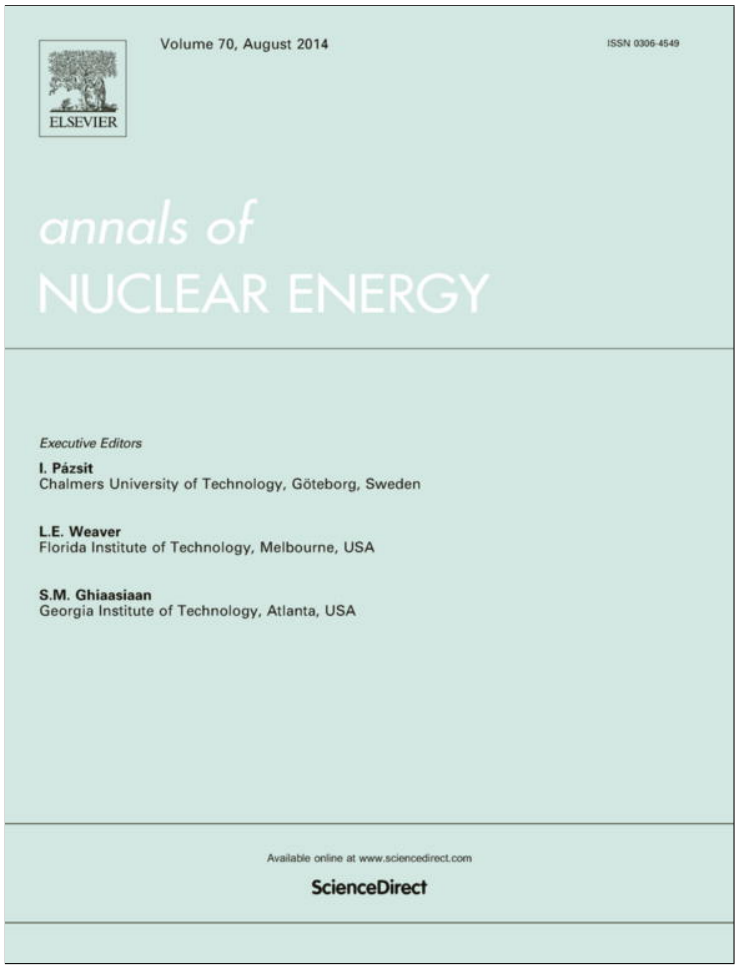

This article appeared in a journal published by Elsevier. The attached copy is furnished to the author for internal non-commercial research and education use, including for instruction at the authors institution and sharing with colleagues.

Other uses, including reproduction and distribution, or selling or licensing copies, or posting to personal, institutional or third party websites are prohibited.

In most cases authors are permitted to post their version of the article (e.g. in Word or Tex form) to their personal website or institutional repository. Authors requiring further information regarding Elsevier's archiving and manuscript policies are encouraged to visit:

http://www.elsevier.com/authorsrights

Author's personal copy

Annals of Nuclear Energy 70 (2014) 147–156

Contents lists available at ScienceDirect

Annals of Nuclear Energy

journal homepage: www.elsevier.com/locate/anucene

Simulation of the behaviour of nuclear fuel under high burnup conditions

Alejandro Soba [a,*], Martin Lemes [a], Martin Emilio González [a], Alicia Denis [a], Luis Romero [b]

[a] U.A. Combustibles Nucleares, Comisión Nacional de Energía Atómica, Avenida del Libertador 8250, 1429 Buenos Aires, Argentina
[b] U.A. Reactores Nucleares, Comisión Nacional de Energía Atómica, Avenida del Libertador 8250, 1429 Buenos Aires, Argentina

ARTICLE INFO

Article history:
Received 10 January 2014
Accepted 3 March 2014
Available online 2 April 2014

Keywords:
DONISIO code
High burnup zone
Gadolinium
Fuel performance modelling

ABSTRACT

In this paper we summarize all the models included in the latest version of the DIONISIO code related to the high burnup scenario. Due to the extension of nuclear fuels permanence under irradiation, physical and chemical modifications are developed in the fuel material, especially in the external corona of the pellet. The codes devoted to simulation of the rod behaviour under irradiation need to introduce modifications and new models in order to describe those phenomena and be capable to predict the behaviour in all the range of a general pressurized water reactor. A complex group of subroutines has been included in the code in order to predict the radial distribution of power density, burnup, concentration of diverse nuclides and porosity within the pellet. The behaviour of gadolinium as burnable poison also is modelled into the code. The results of some of the simulations performed with DIONISIO are presented to show the good agreement with the data selected for the FUMEX I/II/III exercises, compiled in the NEA data bank.
© 2014 Elsevier Ltd. All rights reserved.

1. Introduction

The DIONISIO code has been developed to simulate most of the main phenomena that take place within a fuel rod during the normal operation of a nuclear reactor. The code, which has more than forty interconnected models and a modular structure, predict: temperature distribution, thermal expansion, elastic and plastic strain, creep, irradiation growth, pellet-cladding mechanical interaction, fission gas release, swelling and densification. Axial symmetry is assumed and cylindrical finite elements are used to discretize the domain (Simulación del comportamiento termomecánico de una barra combustible en operación, 2007; Denis and Soba, 2003; Soba and Denis, 2008). The rod is divided into a user defined number of axial segments where a complete axi-symmetric local domain is solved. All the general rod parameters (pressure, fission gas release, free volume of the rod, etc.) are evaluated at the end of every time step averaging the local values obtained. This modification allows taking into account the axial variation of the linear power and, consequently, evaluating the dependence of all the significant rod parameters with that coordinate.

Recently a group of subroutines, designed to extend the application range of the code to high burnup (Kinoshita, 1997; Noirot et al., 2008), has been included. The new calculation tools, which are tuned for UO_2 fuels in LWR conditions, predict the radial distribution of ^{235}U, ^{236}U, ^{238}U, ^{239}Pu, ^{240}Pu, ^{241}Pu and ^{242}Pu across the pellet (Newton and Hutton, 2002). Usually codes specialized in reactor physics perform these calculations solving the Boltzmann transport equations in a number of energy intervals (groups) and including adequate considerations in the region of the resonant absorption peaks of ^{238}U. They predict with high precision the radial distribution of neutron flux, burnup and concentration of every species, fissile, fissionable or fertile, gaseous or solid, within the rod, relevant for the overall process, all of them as functions of time. Among the known reactor codes we mention WIMS-E (Hutton et al., 2004), HELIOS (Stammler et al., 1996; HELIOS Methods, 1998), CONDOR (Eduardo Villarino CONDOR CALCULATION PACKAGE PHYSOR, 2002) and HUEMUL (C. Grant, 2014). Without loosing the required completeness, a simplified treatment consisting in reducing the energy spectrum to a single group was included in DIONISIO. Empirical expressions were obtained to represent, with the higher possible approximation degree, the absorption and capture cross sections as functions of the initial enrichment in ^{235}U, the average burnup and the radial coordinate. The curves obtained with a so drastic simplification demand a testing before incorporation in the general fuel behaviour code. This testing is performed via comparison with the reliable reactor codes. With the validated curves already incorporated, the fuel code is expected to give with a reasonable precision the time evolution of the local burnup and hence, the size of the rim zone. The first antecedent in this type of analysis is found in the RADAR model (HELIOS Methods, 1998) which was validated against the WIMS code. The

* Corresponding author. Tel.: +54 011 4839 6796.
E-mail addresses: soba@cnea.gov.ar (A. Soba), lemes@cnea.gov.ar (M. Lemes), megozal@cnea.gov.ar (M.E. González), denis@cnea.gov.ar (A. Denis), lromero@cnea.gov.ar (L. Romero).

http://dx.doi.org/10.1016/j.anucene.2014.03.004
0306-4549/© 2014 Elsevier Ltd. All rights reserved.

Author's personal copy

TUBRNP model, included in the TRANSURANUS code (Schubert et al., 2008) and the RAPID model (Lee et al., 2000) served as a basis for the development of the present work. The original idea of RADAR is conserved but the validity range and scope of the equations are extended.

The general trend to increasing the fuel initial enrichment originates the need of introducing some absorber material in the core. The usual strategy consisting of including Gd_2O_3 as burnable absorber in the UO_2 matrix has significant effects on the fuel performance: radial modification of the power profile, degradation of the thermal conductivity of the fuel and reduction of the fuel melting point. Among the seven isotopes of gadolinium, those with mass numbers 155 and 157 have particularly high absorption cross section in the thermal energy range. For this reason Gd is burnt in the vicinity of the fuel surface thus shielding the pellet interior from thermal neutrons. The interface between burnt and unburnt Gd shifts towards the pellet centre as irradiation progresses. The isotopes with mass numbers 156 and 158 produced respectively by these reactions have very small absorption cross sections and need not any further consideration from the neutron distribution point of view (Massih et al., 1992). We include the possibility of simulating UO_2 pellets doped with Gd_2O_3 as a burnable poison obtaining the evolution of these isotopes across the pellet radius.

The task described in the preceding paragraph was performed in connection with the reactor cell codes HUEMUL and CONDOR. In Section 2 we describe some of the characteristics of this work and present some results, taking into the account that the main task and detailed description were presented elsewhere (Soba et al., 2013).

Additionally, an expression to describe the burnup induced degradation of the thermal conductivity of UO_2 during the fuel operation time was recently elaborated. The formula also evaluates the conductivity of fuels with some content of Gadolinium in the range from 0 to 8 wt%, which is the usual proportion in the UO_2 fuels with burnable poisons. The new model was firstly compared with conductivity experimental data and was then implemented into the DIONISIO code. Some results of this code aspect were reported in González et al. (2013).

Moreover, empirical expressions representing the amounts of Caesium, Neodymium and Xenon, mainly following Lassmann et al. (1995, 2003) were compared with experimental data and incorporated in DIONISIO as new subroutines.

Finally new models which describe the porosity behaviour and fission gas release in the rim are also developed and included in the code. This work was presented elsewhere (Martín Lemes et al., 2014; Estudio analítico y numérico de los efectos de la irradiación hasta alto quemado en combustibles de reactores de potencia, 2013) but for completeness all the models referred to HBS are presented here. The main aspects are summarized in Section 4 along with some results of comparisons with several experimental data taken from the literature to show the overall performance of the code.

These improvements together with the structural modifications of the program gave origin to the new code version DIONISIO 2.0. Moreover, a considerable number of experiments compiled in IAEA (http://www.iaea.org., 2014; http://www.oecd-nea.org/science/fuel/ifpelst.html., 2014) data bases were simulated with the present code structure. Some of these comparisons are also presented here.

2. One energy group calculation

The balance equations listed below express the variation rate of the concentration of each of the relevant isotopes. They are indicated by N, measured in $atoms/cm^3$, with a subscript formed by the name of the element and the mass number of the isotope. σ and ϕ represent, respectively, the cross section (expressed in barns) and the neutron flux (in $neutrons/(cm^2\,s)$), assuming the energy spectrum reduced to a single group. σ is labeled with a subscript a, c or f to indicate absorption, capture or fission, respectively, and with a superscript to identify the nuclide. The same superscript is used to label the decay constant λ (measured in $1/s$). N and ϕ are considered as functions of the irradiation time (t) and the radial position (r) in the pellet. For the U and Pu isotopes, the cross sections are assumed to depend on the radius, the average burnup (b) and the initial enrichment (q) in ^{235}U measured in $w\%$. For the Gd isotopes, these parameters depend also on the initial content of Gd (g), measured in $w\%$.

$$\frac{\partial C_{U235}}{\partial t} = -C_{U235}(t,r)\sigma_a^{235}(b,r)\phi(t,r) \tag{1}$$

$$\frac{\partial C_{U236}}{\partial t} = -C_{U236}(t,r)\sigma_a^{236}(b,r)\phi(t,r) + C_{U235}(t,r)\sigma_c^{235}(b,r)\phi(t,r) \tag{2}$$

$$\frac{\partial C_{U238}}{\partial t} = -C_{U238}(t,r)\sigma_a^{238}(b,r)\phi(t,r) \tag{3}$$

$$\frac{\partial C_{Pu239}}{\partial t} = -C_{Pu239}(t,r)\left(\sigma_a^{239}(b,r)\phi(t,r) + \lambda^{239}\right) + C_{U238}(t,r)\sigma_c^{238}(b,r)\phi(t,r) \tag{4}$$

$$\frac{\partial C_{Pu240}}{\partial t} = -C_{Pu240}(t,r)\left(\sigma_a^{240}(b,r)\phi(t,r) + \lambda^{240}\right) + C_{Pu239}(t,r)\sigma_c^{239}(b,r)\phi(t,r) \tag{5}$$

$$\frac{\partial C_{Pu241}}{\partial t} = -C_{Pu241}(t,r)\left(\sigma_a^{241}(b,r)\phi(t,r) + \lambda^{241}\right) + C_{Pu240}(t,r)\sigma_c^{240}(b,r)\phi(t,r) \tag{6}$$

$$\frac{\partial C_{Pu242}}{\partial t} = -C_{Pu242}(t,r)\left(\sigma_a^{242}(b,r)\phi(t,r) + \lambda^{242}\right) + C_{Pu241}(t,r)\sigma_c^{241}(b,r)\phi(t,r) \tag{7}$$

$$\frac{\partial C_{Gd155}}{\partial t} = -C_{Gd155}(t,r)\sigma_a^{155}(r,b,q,g)\phi(t,r) \tag{8}$$

$$\frac{\partial C_{Gd157}}{\partial t} = -C_{Gd157}(t,r)\sigma_a^{157}(r,b,q,g)\phi(t,r) \tag{9}$$

Reactor codes generally divide the neutrons energy spectrum in two groups, described as thermal (neutrons with energies below *0.65* eV) and fast (neutrons with higher energies). Both the fast and thermal fluxes are used in the balance Eqs. (1)–(9) to predict the behaviour of each species.

The increased content of Plutonium in the external zone is basically due to the behaviour in the resonance region of the absorption cross section of ^{238}U. The equation used in DIONISIO to express this behaviour was fitted to results of simulations performed with the CONDOR and HUEMUL codes:

$$\sigma_{abs}^{238}(r,b,en) = c_1\left(c_2 + c_3 b_{1000} + c_4 b_{1000}^2 + c_5 b_{1000}^3\right) \times \left(c_6 + c_7 \exp\left(c_8\left(1 - \frac{r}{r_{\max}}\right)^{c_9}\right)\right) \tag{10}$$

The function has a shape similar to the expressions used in other codes (Lee et al., 2000). The remaining cross section functions to be introduced in the subroutine are evaluated as follows: the codes CONDOR and HUEMUL are run assuming the conditions of a generic UO_2 pellet; the initial enrichment is varied from 0.7% to 12%; the initial content of Gd (g) is assigned values in the range 4–10%; the final average burnup is given values ranging from fresh fuel to 120 MWd/kgU. With these results, curves are drawn for

Author's personal copy

Table 1
Correlation formulae and the corresponding coefficients for the absorption cross section of ^{235}U, ^{236}U, ^{240}Pu, ^{242}Pu, ^{155}Gd and ^{157}Gd calculated for a single energy group.

$\sigma_a^{235} = f_1(r,b,q,g=0)$, Eq. (11), with
$a_0 = 8.5663\times10^{+01} - 1.452\times10^{+01}q + 7.9068\times10^{-01}q^2$
$a_1 = -9.3400\times10^{-04} + 4.5791\times10^{-04}q - 8.1504\times10^{-06}q^2 + 5.7252\times10^{-07}q^3 - 1.2767\times10^{-07}q^4$
$a_2 = 1.3955\times10^{+01} + 4.4988\times10^{-01}q$
$a_3 = 5.9610\times10^{-09} - 2.6213\times10^{-09}q + 5.5749\times10^{-10}q^2 - 3.3465\times10^{-11}q^3$
$a_4 = -5.8722\times10^{+01} - 2.8297q$
$a_5 = -5.7726\times10^{-14} + 4.700\times10^{-14}q - 1.4529\times10^{-14}q^2 + 1.7064\times10^{-15}q^3 - 6.7250\times10^{-17}q^4$
$a_6 = 1.1990\times10^{+02} + 4.6660q - 1.2529\times10^{-01}q^2$
$a_7 = -1.0488\times10^{-05} + 1.4527\times10^{-07}q + 2.6736\times10^{-06}q^2 - 2.0278\times10^{-07}q^3$
$a_8 = 1.2862\times10^{-10} + 7.3720\times10^{-11}q - 2.6430\times10^{-11}q^2 + 1.6497\times10^{-12}q^3$
$a_9 = -3.0515\times10^{-05} - 6.0782\times10^{-06}q - 2.5616\times10^{-06}q^2 + 6.0349\times10^{-07}q^3 - 2.9614\times10^{-08}q^4$
$\sigma_a^{236} = f_1(r,b,q,g=0)$, Eq. (11), with
$a_0 = 1.6057 - 6.8713q + +9.6081\times10^{-01}q^2 - 4.6908\times10^{-02}q^3 - 1.0528\times10^{-05}q^4$
$a_1 = 9.7599\times10^{-02} - 6.8512\times10^{-02}q + 2.1897\times10^{-02}q^2 - 2.8643\times10^{-03}q^3 + 1.3365\times10^{-04}q^4$
$a_2 = 4.6102\times10^{+01} + 7.6858\times10^{+01}q - 1.2920\times10^{+01}q^2 + 9.6226\times10^{-01}q^3 - 2.6040\times10^{-02}q^4$
$a_3 = -2.2220\times10^{-03} + 8.3287\times10^{-04}q - 1.8398\times10^{-04}q^2 + 1.8434\times10^{-05}q^3 - 6.7646\times10^{-07}q^4$
$a_4 = -1.7051\times10^{+02} - 2.7093\times10^{+02}q + 4.9345\times10^{+01}q^2 - 4.1398q^3 + 1.3432\times10^{-01}q^4$
$a_5 = 1.21073\times10^{-05} - 1.3072\times10^{-06}q + 8.4640\times10^{-08}q^2$
$a_6 = 1.9650\times10^{+02} + 2.9111\times10^{+02}q - 5.6125\times10^{+01}q^2 + 5.0616q^3 - 1.7933\times10^{-01}q^4$
$a_7 = 1.1519\times10^{-01} - 1.1481\times10^{-03}q - 4.3180\times10^{-02}q^2 + 8.5555\times10^{-03}q^3 - 4.8473\times10^{-04}q^4$
$a_8 = -5.0679\times10^{-04} - 9.1153\times10^{-04}q + 3.2156\times10^{-04}q^2 - 4.4494\times10^{-05}q^3 + 2.1812\times10^{-06}q^4$
$a_9 = -1.0871\times10^{-01} + 2.1636\times10^{-01}q - 6.5612\times10^{-03}q^2 - 3.2417\times10^{-03}q^3 + 2.6291\times10^{-04}q^4$
$\sigma_a^{240} = f_1(r,b,q,g=0)$, Eq. (11), with
$a_0 = 2.4356\times10^{+02} - 7.4465\times10^{+01}q + 2.0205\times10^{+01}q^2 - 2.3110q^3 + 9.0858\times10^{-02}q^4$
$a_1 = -5.4351\times10^{-03} - 3.5277\times10^{-04}q + 1.2257\times10^{-04}q^2 - 9.4641\times10^{-06}q^3 + 2.7345\times10^{-07}q^4$
$a_2 = -9.0926\times10^{+01} + 5.6823\times10^{+02}q - 1.5718\times10^{+02}q^2 + 1.7378\times10^{+01}q^3 - 6.7179\times10^{-01}q^4$
$a_3 = 6.2413\times10^{-08} + 4.1771\times10^{-09}q - 1.6026\times10^{-09}q^2 + 1.2766\times10^{-10}q^3 - 3.7148\times10^{-12}q^4$
$a_4 = -8.3656\times10^{+01} - 1.9650\times10^{+03}q + 5.4960\times10^{+02}q^2 - 6.0663\times10^{+01}q^3 + 2.3410q^4$
$a_5 = -2.4281\times10^{-13} + 1.4976\times10^{-14}q$
$a_6 = 6.59769\times10^{+02} + 1.9983\times10^{+03}q - 5.7275\times10^{+02}q^2 + 6.3522\times10^{+01}q^3 - 2.4543q^4$
$a_7 = 3.9184\times10^{-03} - 3.0028\times10^{-03}q + 7.9302\times10^{-04}q^2 - 9.0454\times10^{-05}q^3 + 3.5730\times10^{-06}q^4$
$a_8 = -2.1097\times10^{-08} - 1.0837\times10^{-09}q + 2.8649\times10^{-11}q^2 + 3.4214\times10^{-11}q^3 - 2.0635\times10^{-12}q^4$
$a_9 = -4.2931\times10^{-04} + 4.8312\times10^{-03}q - 1.1840\times10^{-03}q^2 + 1.2638\times10^{-04}q^3 - 4.8460\times10^{-06}q^4$
$\sigma_a^{242} = f_1(r,b,q,g=0)$, Eq. (11), with
$a_0 = 3.0118\times10^{+01} - 6.5618\times10^{-01}q$
$a_1 = 7.3847\times10^{-02} - 7.2747\times10^{-02}q + 2.7282\times10^{-02}q^2 - 3.1957\times10^{-03}q^3 + 1.1832\times10^{-04}q^4$
$a_2 = 6.4450 + 2.1587\times10^{-01}q - 2.4665\times10^{-02}q^2$
$a_3 = -4.0275\times10^{-04} - 2.8568\times10^{-04}q + 2.5461\times10^{-05}q^2$
$a_4 = -2.7537\times10^{+01} + 7.4897\times10^{-01}q$
$a_5 = 4.1927\times10^{-06} + 4.0962\times10^{-07}q - 6.7322\times10^{-08}q^2$
$a_6 = 3.0368\times10^{+01} - 5.8145\times10^{-01}q$
$a_7 = 9.7741\times10^{-03} - 2.0036\times10^{-02}q + 1.1978\times10^{-03}q^2$
$a_8 = -5.1067\times10^{-04} + 1.5204\times10^{-04}q - 7.4631\times10^{-06}q^2$
$a_9 = 1.5474\times10^{-01} - 1.1565\times10^{-03}q - 5.4451\times10^{-04}q^2$
$\sigma_a^{155} = f_1(r,b,q,g)$, Eq. (11), with
$a_0 = 1.9339\times10^{+02} - 1.2885\times10^{+01}\cdot q - 7.831\cdot g$
$a_1 = 1.4676\times10^{+02} - 3.0342\times10^{+01}\cdot q - 3.3965\times10^{+01}\cdot g + 2.7774\cdot q^2 + 2.6193\cdot g^2$
$a_2 = -2.5837\times10^{+03} + 3.4162\times10^{+02}\cdot q + 2.5883\times10^{+02}\cdot g$
$a_3 = \frac{q\,g}{(-7.1656\times10^{-01} + 4.4941\times10^{-02}\cdot exp(q) + 6.7029\times10^{-03}\cdot exp(g))}$
$a_4 = -1.1637\times10^{+04} + 5.8691\times10^{+03}\cdot q + 2.6127\times10^{+03}\cdot g - 1.1681\times10^{+03}q^2 -$
$3.1771\times10^{+02}\cdot g^2 + 7.5772\times10^{+01}\cdot q^3 + 7.6019\cdot g^3 - 9.1283\times10^{+02}q\cdot g +$
$3.3483\times10^{+01}q^2\cdot g + 4.5734\times10^{+01}\cdot g^2\cdot q$
$a_5 = -9.2356\times10^{-01} + 6.6888\times10^{-02}\cdot q + 1.0511\times10^{-01}\cdot g$
$a_6 = -8.3028\times10^{+02} + 2.9518\times10^{+03}\cdot q + 1.8994\times10^{+03}\cdot g - 1.9336\times10^{+02}\cdot q^2$
$-7.2757\times10^{+01}\cdot g^2 + 2.3589\times10^{+01}\cdot q\cdot g$
$a_7 = 8.9867\times10^{+02} - 6.5205\times10^{+01}\cdot q - 4.5833\times10^{+02}\cdot g$
$a_8 = -4.1393\times10^{+01} + 9.0863\times10^{-01}\cdot q + 4.9750\cdot g + 1.2383\times10^{-01}\cdot q^2 - 2.4634\times10^{-01}\cdot g^2$
$a_9 = -8.0211\times10^{+02} + 6.0288\times10^{+01}\cdot q + 6.2367\times10^{+01}\cdot g$
$\sigma_a^{157} = f_1(r,b,q,g)$, Eq. (11), with
$a_0 = 7.3318\times10^{+03} - 6.7731\times10^{+03}\cdot q + 1.6764\times10^{+03}\cdot g + 1.5868\times10^{+03}\cdot q^2 -$
$1.7375\times10^{+02}\cdot g^2 - 1.0986\times10^{+02}\cdot q^3 + 5.7503\cdot g^3 - 2.4407\times10^{+02}\cdot q\cdot g$
$+8.8016\cdot q^2\cdot g + 1.1284\times10^{+01}\cdot g^2\cdot q$
$a_1 = 6.4762\times10^{+02} - 1.3052\times10^{+02}\cdot q - 1.5197\times10^{+02}\cdot g + 1.1948\times10^{+01}\cdot q^2 + 1.169\times10^{+01}\cdot g^2$
$a_2 = -1.1121\times10^{+04} + 1.4610\times10^{+02}\cdot q + 1.1090\times10^{+03}\cdot g$

(*continued on next page*)

Author's personal copy

$$a_3 = \frac{q\,g}{(-1.7177\times10^{-01}+1.0722\times10^{-02}\cdot exp(q)+1.5135\times10^{-03}\cdot exp(g))}$$
$$a_4 = 1.7696\times10^{+04} - 5.5024\times10^{+03}\cdot q - 5.0299\times10^{+03}\cdot g$$
$$a_5 = -1.3180\times10^{+01} + 1.3711\cdot q + 3.3317\cdot g - 1.0730\times10^{-01}\cdot q^2 - 2.3917\times10^{-01}\cdot g^2$$
$$a_6 = 1.9835\times10^{+04} + 4.9922\times10^{+03}\cdot q + 4.9244\times10^{+03}\cdot g$$
$$a_7 = 3.8504\times10^{+03} - 2.7806\times10^{+02}\cdot q - 1.9614\times10^{+02}\cdot g$$
$$a_8 = -1.6426\times10^{+02} - 5.1839\times10^{-01}\cdot q + 2.1626\times10^{+01}\cdot g + 8.9344\times10^{-01}\cdot q^2 - 1.097\cdot g^2$$
$$a_9 = -4.2786\times10^{+03} + 5.5727\times10^{+02}\cdot q + 3.3387\times10^{+02}\cdot g - 2.9959\times10^{+01}\cdot q^2 - 5.5259\cdot g^2$$

each of the relevant species for the absorption and capture cross sections, thermal and fast neutron flux and local burnup end in case of ^{155}Gd and ^{157}Gd in terms of the initial gadolinium contents. Then empirical expressions are fitted for the cross sections as functions of the burnup, the radial coordinate and the enrichment, for each of the species. In this way, the so generated expressions are valid in a continuous range limited by the boundary values of the parameters mentioned above. These functions, which we indicate as $\sigma^i_{a,c}(r,b,q,g)$, are introduced in DIONISIO and subjected to several tests: firstly, the parameterized functions are compared with the curves obtained with the reactor codes; secondly, the predictions of the balance Eqs. (1)–(10) are compared with those of the reactor physics codes; finally, experimental results are used to compare the performance of DIONISIO as a whole.

The formulae fitted in the present work for the cross sections of absorption, capture and fission of ^{235}U, ^{236}U, ^{238}U, ^{239}Pu, ^{240}Pu, ^{241}Pu, ^{242}Pu, ^{155}Gd and ^{157}Gd can be grouped in the following general function shape:

$$f_1(r,b,q) = a_0 + a_1 r + a_2 b + a_3 r^2 + a_4 rb + a_5 b^2 + a_6 r^3 + a_7 r^2 b + a_8 rb^2 + a_9 b^3 \quad (11)$$

The following step is fitting empirical expressions for the coefficients $a_0,\ldots,a_9$ of (11) in terms of q and g for gadolinium. In this way, the cross sections of both gadolinium isotopes depend on four variables. To determine the total neutron flux, necessary to solve the balance Eqs. (1)–(9), a parametric expression is built in terms of the initial content of ^{235}U and Gd, the average burnup and the linear power in the pellet.

$$\phi_{tot}(r,b,q,g) = \frac{P_{vol}}{3.2\times10^{11}\sum_i \sigma^i_f(r,0,1,g)N_i} \times (a_0 + a_1 b + a_2 q + a_3 b^2 + a_4 bq + a_5 q^2 + a_6 b^3 + a_7 b^2 q + a_8 bq^2 + a_9 q^3) \quad (12)$$

where P_{vol} is the volumetric power density expressed in W cm^{-3}, $\sigma^i_f(r,0,1,g)$ represents the fission cross section of isotope i (i = 155 or 157) in the reference condition corresponding to fresh fuel (b = 0), enrichment 1 wt% (q = 1) and initial gadolinium content (g).

2.1. Comparison between predicted and calculated cross sections

The empirical expressions obtained for σ_f^{235}, σ_a^{238}, σ_a^{239} and σ_a^{241} (representing the fission cross section of ^{235}U and the absorption cross sections of ^{238}U, ^{239}Pu and ^{241}Pu, respectively) and those for ϕ_{tot} where published elsewhere (Soba et al., 2013). In this paper we present, as examples, the empirical expressions obtained for σ_a^{235}; σ_a^{236}; σ_a^{240} and σ_a^{242} (representing the absorption cross section of ^{235}U, ^{236}U, ^{240}Pu and ^{242}Pu, respectively) and those coefficients for $\sigma_a^{155}(r,b,q,g)$, $\sigma_a^{157}(r,b,q,g)$ referred to the absorption cross section of Gadolinium isotopes. All these functions are displayed in Table 1.

Figs. 1–5 show, under selected conditions, the comparison between the empirical laws fitted in this work and the results obtained with the reactor codes HUEMUL and CONDOR for the local burnup, concentration and cross sections of absorption, capture and fission of the *U* and *Pu* isotopes.

2.2. Comparison against experimental results

Experimental data corresponding to the high burnup range were chosen from the NEA data bank to compare the code results with the numerical predictions. In particular, experimental determinations of the total *U* and *Pu* content are found in several HBEP (High Burnup Effects Programme Final Report, 2002) experiments, an international series of experiences with the objective of obtaining useful and well-characterized data on rods irradiated to high burnup levels. We present in Fig. 6 a comparison between experimental data and predictions of DIONISIO for the A3/6-4 and 3-189 rods.

The following figures (Fig. 7) show the measured data of average burnup and total plutonium together with the results of DIONISIO. The experiments were taken from the FUMEX II (IAEA, 2012) and FUMEXIII (Killeen et al., 2009) databasis.

In Fig. 8 we present some DIONISIO calculations of Gadolinium isotopes content in function of burnup (left graph) and across de

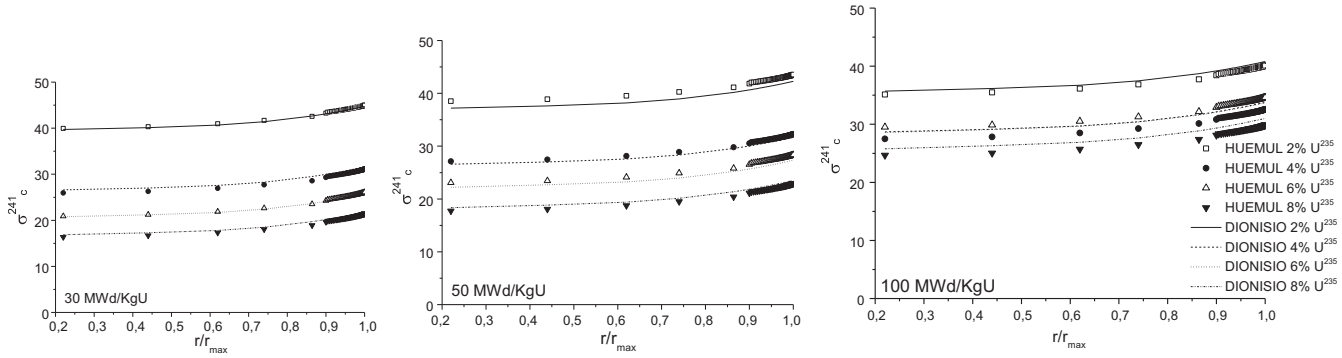

Fig. 1. Capture cross section σ_c^{241} of ^{241}*Pu* vs. the relative radius for different values of the initial enrichment and different levels of average burnup. Comparison between the values predicted by HUEMUL and the functions included in DIONISIO.

Author's personal copy

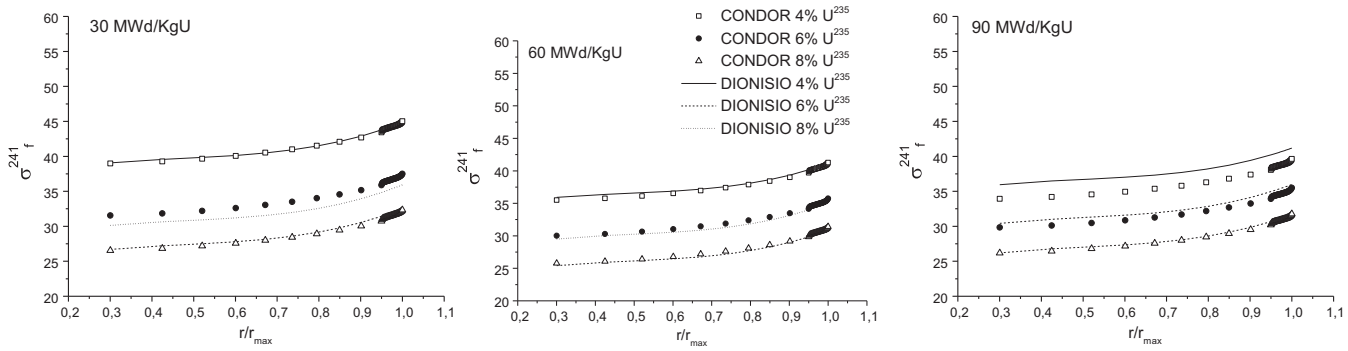

Fig. 2. Fission cross section σ_f^{241} of ^{241}Pu vs. the relative radius for different values of the initial enrichment and different levels of average burnup. Comparison between the values predicted by CONDOR and the functions included in DIONISIO.

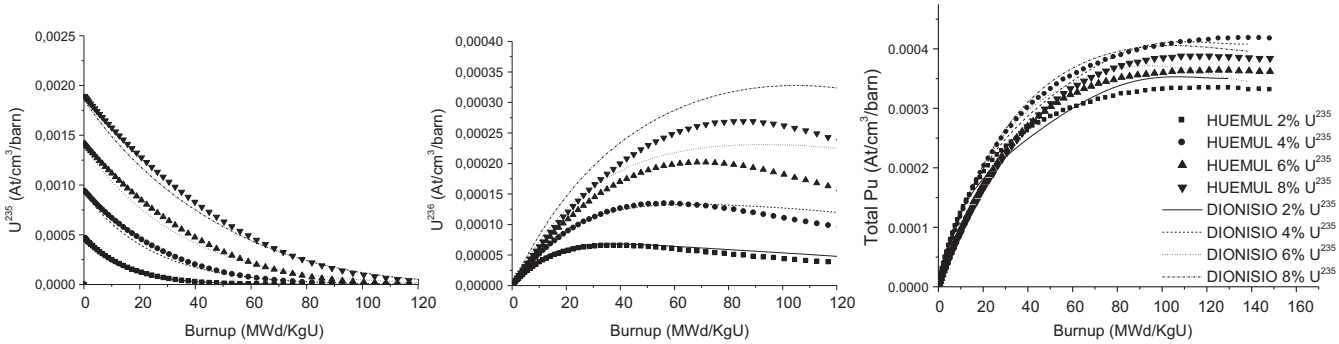

Fig. 3. Concentration of U^{235}, U^{236} and total Pu predicts by HUEMUL and DIONISIO, in function of burnup for different enrichments in he central point of the pellet ($r/r0 \sim 0.5$).

pellet (right graph). The data for comparison were taken from reference (Massih et al., 1992).

3. Other species calculations

The experimental determinations (Lassmann et al., 1995) show that the fission yield of Cs, Nd and Xe can be reasonably approximated by constants, so that the generation rates of these elements per unit volume (involving the different isotopes and their decay chains) are proportional to the fission rate. The rate laws are thus expressed as $\frac{\partial C_i}{\partial t} = Y_i \dot{f}$ where i indicates the element, C is the concentration in atoms/cm^3, $\dot{f}$ is the local fission rate in fissions/(cm^3 s) and the respective fission yields are $Y_{Cs} \approx 0.150$, $Y_{Nd} \approx 0.199$ and $Y_{Xe} \approx 0.268$. These expressions are used in the TRANSURANUS code and were also adopted in DIONISIO.

The proportionality between the local concentration of *Nd* and the local burnup is experimentally verified. Something similar also holds for *Cs*, but with a larger dispersion. Due to this property, *Nd* and *Cs* concentrations are used as a measure of the local burnup level. With respect to xenon, the EPMA determinations show the decrease of the gas dissolved in the matrix for burnups higher that a certain level. *Xe* concentration is experimentally used to locate the burnup threshold Bu_o. For $Bu > Bu_o$, the high-burnup microstructure forms, and a considerable fraction of *Xe* is collected by the large pores. The depletion of gas from the matrix is well represented by the following empirical expression (Lassmann et al., 1995) which was adopted for the concentration of Xe dissolved in the matrix

$$C_{Xe} = 1.46 \times 10^{-2}\left(\left(\frac{1}{\alpha}\right) + \left(Bu_o - \left(\frac{1}{\alpha}\right)\right)e^{-\alpha(Bu-Bu_o)}\right) \quad (13)$$

where $\alpha = 0.058$ is a fitting parameter. These expressions are compared with experimental data. In particular, the determinations performed on the A3-6-4 rod of the HBEP3 experiment are shown in Fig. 9 and compared with the curves obtained with this approximation.

Fig. 10 presents an extensive comparison between Cesium experimental measurements and values calculated with DIONISIO in some rods of the HBEP (High Burnup Effects Programme Final Report, 2002), OSIRIS(Rapport d'Assurance Qualite Crayon FF06E2BV/G07/1067, 1998) and REGATE(NEA, 2004) experiments. A general trend of DIONISIO to overestimating the experimental values in the range of low Cs production is recognized. Nevertheless, the 90% of the data analyzed fall within the 15% error lines.

4. Thermal conductivity of UO_2 and (U,Gd)O_2

Computer codes used for simulating the thermo-mechanical behaviour of nuclear fuels must include an adequate description of the thermal conductivity, since it plays a key role on the accuracy of the prediction of temperature distribution in the system, and in consequence of all the physical properties of the whole system. The thermal conductivity of UO_2 is a function not only of temperature, but of variables such as burnup level, porosity, stochiometry, *Pu* and *Gd* content, etc.

In this work, different thermal conductivity models published in the open literature have been evaluated, for UO_2, (U,Pu)O_2 and (U,Gd)O_2 fuels, as well as a large amount of related experimental data. Staring from an expression published by Fink (Fink, 2000), modifications were introduced to reflect the degradation of thermal conductivity due to burnup and to the presence of *Gd* in the lattice and to give the best possible fitting to the experimental data available in the literature. The expression adopted is (in W/cm °C)

$$k(T) = (1-p^{2/3})\left[\frac{1}{A + BT + CT^2 + a_{Gd}w_{Gd}(b_{Gd} - T) + h_D(T, Bu)} + (1 - c_{Gd}w_{Gd})\frac{D}{T^{5/2}}\exp\left(-\frac{E}{T}\right)\right] \quad (14)$$

Author's personal copy

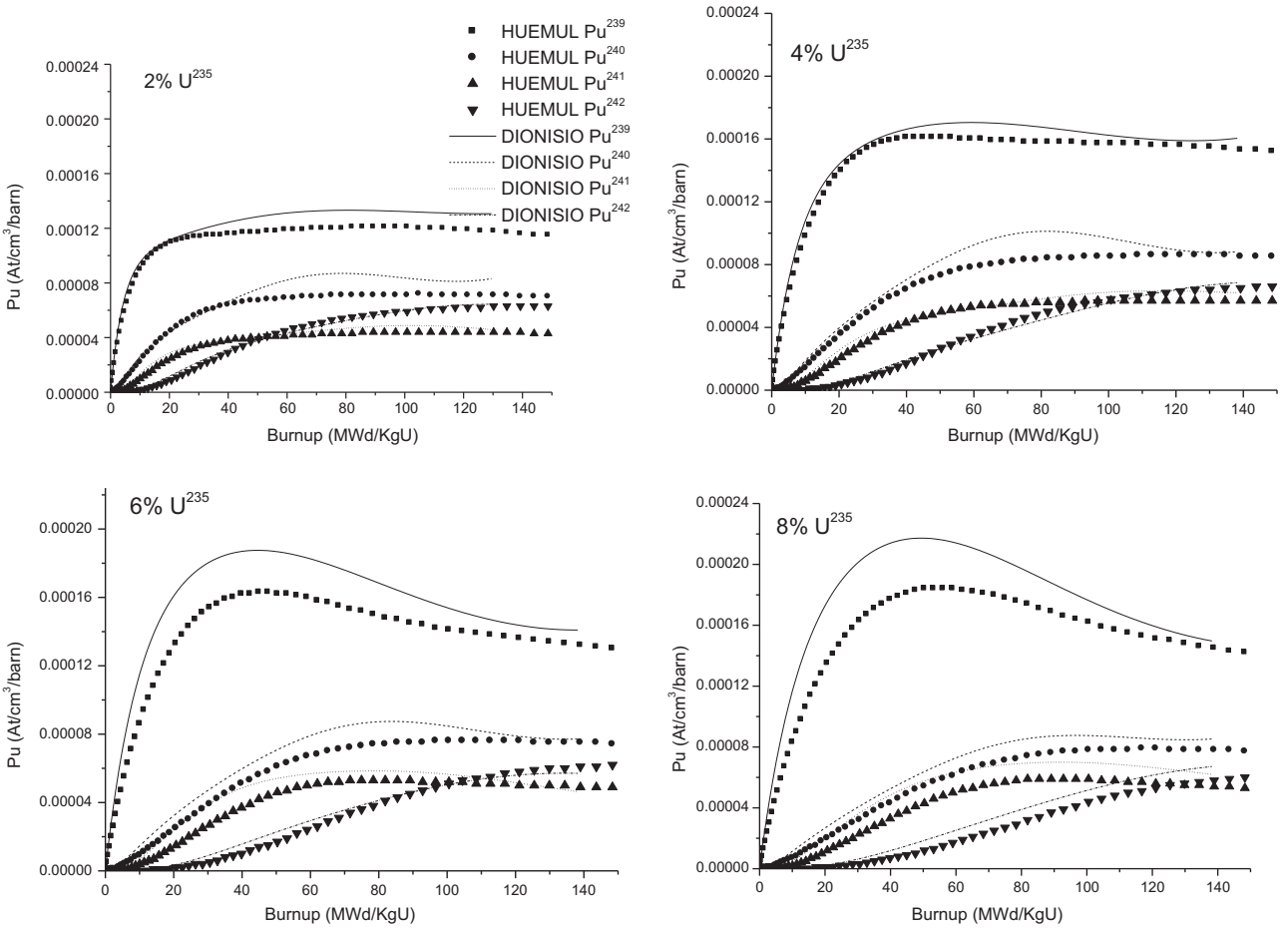

Fig. 4. Concentration of ^{239}Pu, ^{240}Pu, ^{241}Pu and ^{242}Pu vs. burnup for different values of the initial enrichment, predicted by HUEMUL and DIONISIO, for $r/r_{max} \approx 0.85$.

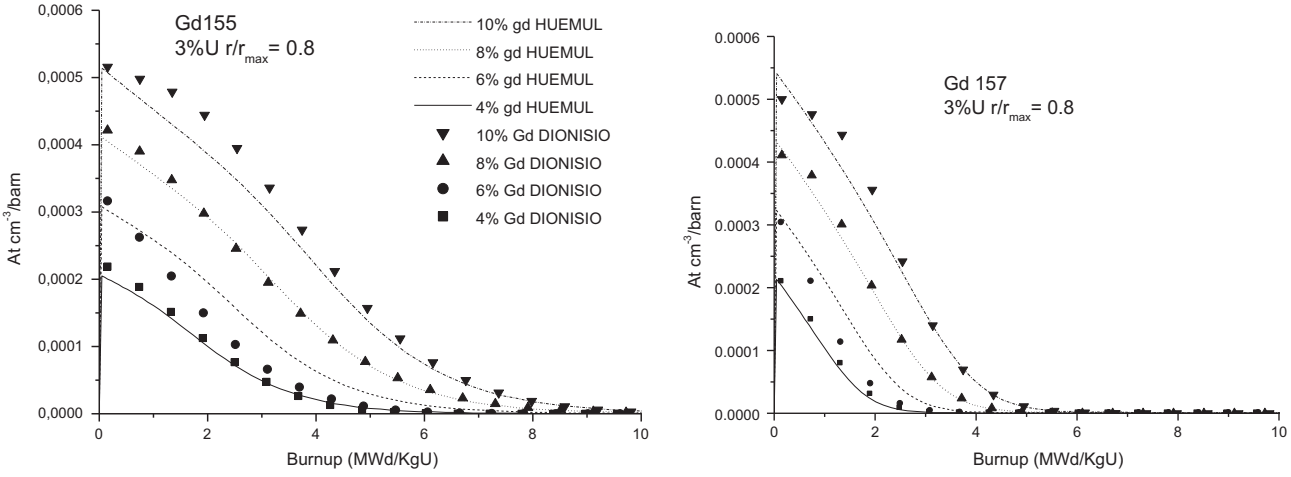

Fig. 5. Concentration of ^{155}Gd and ^{157}Gd as a function of burnup for $r/r_{max} \approx 0.80$. Case 3% ^{235}U.

where p is the material porosity, T the absolute temperature, w_{Gd} the weight fraction of *Gd*. For the function h_D was adopted the expression (Spino et al., 2005)

$$h_D(Bu) = A_D + B_D \exp\left(-\frac{Bu}{C_D}\right) \tag{15}$$

The fitting parameters of this formula as well as a_{Gd}, b_{Gd} and c_{Gd} in the previous one were selected according to the experimental data compiled in references (Fink, 2000; Ronchi et al., 2004). Fig. 11 shows the effect of burnup on the thermal conductivity of UO_2. Generally speaking, in the range 0–1660 °C, different authors' proposals are similar evidencing the decrease of conductivity with temperature. For higher temperatures there is a tendency to grow and the dispersion is clearly larger. While the effect of burnup is more visible in the lower temperature range, for temperatures about 1600 °C and $Bu > 60$ MWd/kgU the conductivity is about 0.02 W/cm°C.

Fig. 12 shows the addition of gadolinium effect on thermal conductivity of unirradiated UO_2. The conductivity degradation increases with the *Gd* content, although its influence is relatively lower for high temperatures and burnup levels.

Author's personal copy

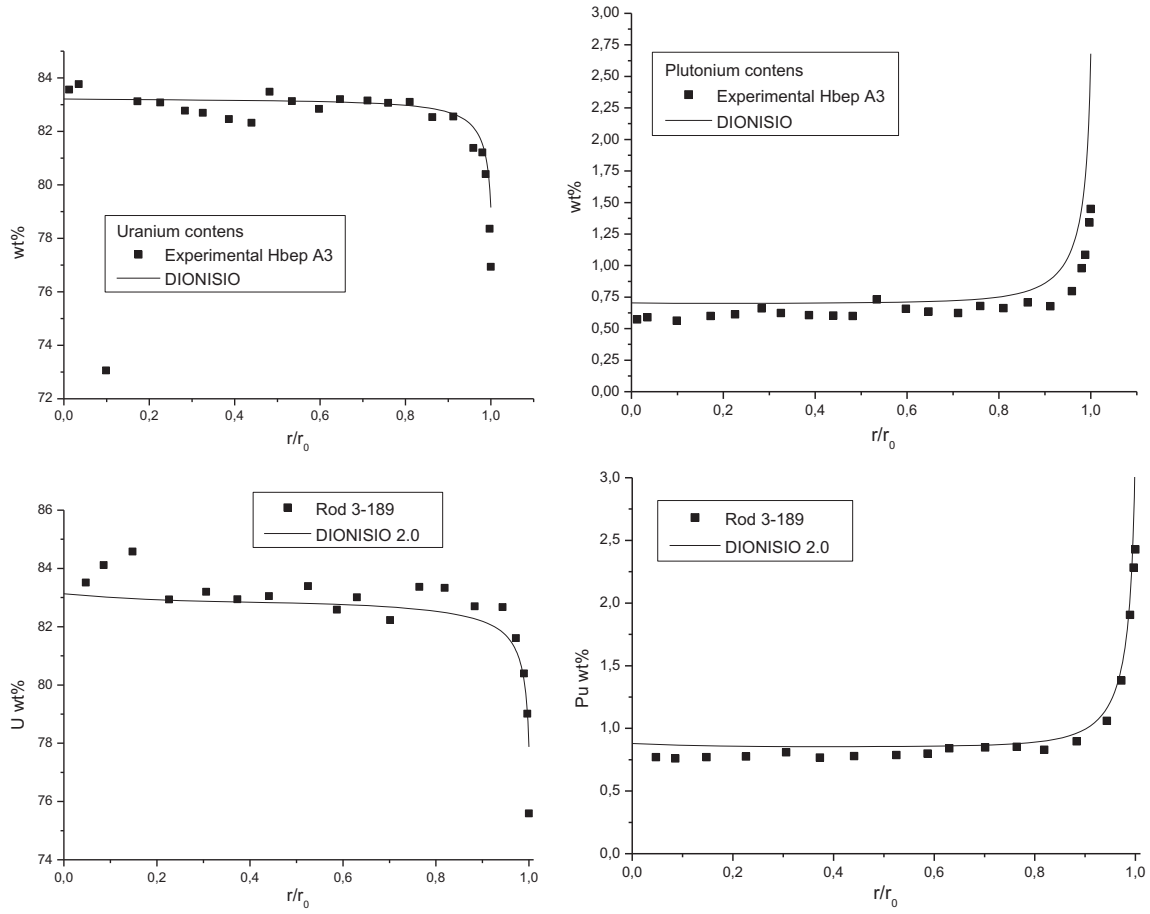

Fig. 6. Total plutonium and Uranium across the pellet radio in HBEP A3 experiment (High Burnup Effects Programme Final Report, 2002).

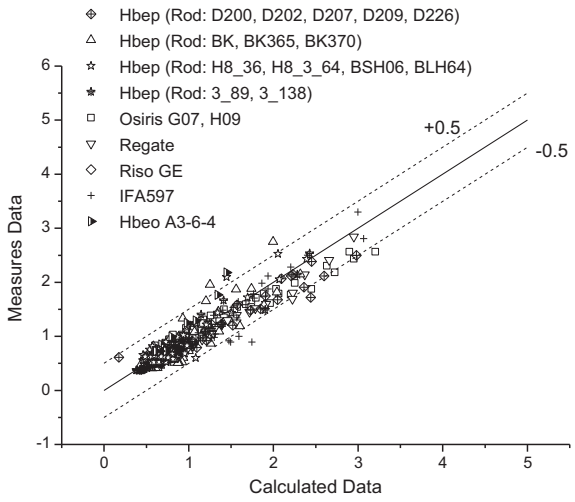

Fig. 7. Total plutoniun measured vs. calculated. Experiments taken from HBEP-3(High Burnup Effects Programme Final Report, 2002), Regate(NEA, 2004), RIso-GE(IFPE, 1995), Osiris-G07/H09(Rapport d'Assurance Qualite Crayon FF06E2BV/G07/1067, 1998; Rapport d'Assurance Qualite Crayon FF0EFELX/H09/5007, 1998).

5. A model to predict porosity evolution in rim zone

For extended irradiation periods, a new microstructure develops in the pellet periphery (rim zone) characterized by small grains and large pores as compared with those of the original material. In this region xenon is absent from the solid lattice (although it continues to be dissolved in the rest of the pellet). The porous microstructure in the pellet edge causes local changes in the mechanical and thermal properties, thus affecting the overall fuel behaviour. The evolution of porosity in the high burnup structure (HBS) is assumed to be determinant of the retention capacity of the fission gases released by the matrix. This is the reason why, during the latest years a considerable effort has been devoted to characterizing the parameters that influence porosity.

Starting from several works published in the open literature, a model was developed to describe the behaviour and development of porosity at local burnup values ranging from 60 to 300 MWd/KgHM. The model is mathematically expressed by a system of non-linear differential equations. Phenomena like the growth of pore radius by vacancies trapping, the interactions of different orders between open and closed pores (coalescence), the evolution of the pore number density, the internal pressure and over pressure within the closed pores, interactions between pores and the free surface (gas venting), the fission gas retained in the matrix and released to the closed pores and to the free volume of the rod are analyzed.

The HBS can be conventionally considered to start at ≈60 MWd/kgU. Two parameters, porosity and pore number density, become useful to describe the HBS. Both show a change of behaviour at a burnup threshold of about 100 MWd/kgU. In the interval between 60 and 100 MWd/kgU, porosity increases with burnup at a rate of about 1.7%/10 MWd/kgU until it reaches about 10% at the burnup critical value. For burnups higher than 100 MWd/kgU, the porosity increase rate is about 0.6%/10 MWd/kgU (Spino et al., 2006). The pore number density, instead, increases with burnup until reaching a maximum of about 10^8 pores/mm^3 at the burnup threshold value

Author's personal copy

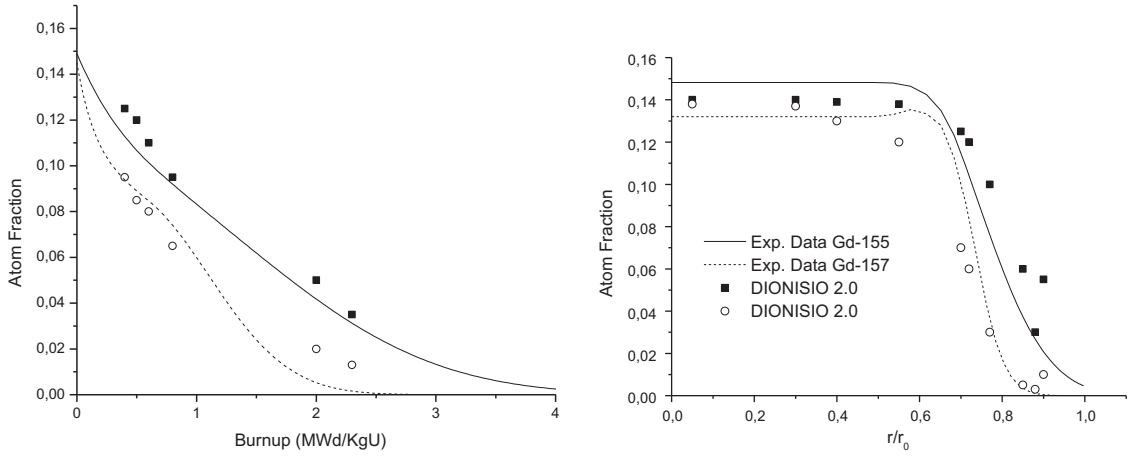

Fig. 8. Gadolinium isotopes evolution in function of burnup (left) and across de pellet (right). Data were taken from Massih et al. (1992).

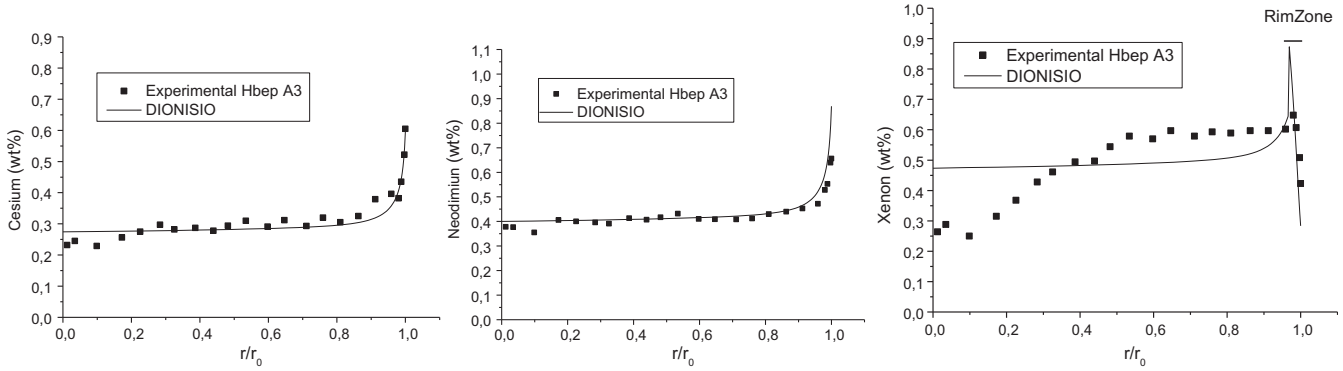

Fig. 9. Local concentration of (a) Cs, (b) Nd and (c) Xe measured in the rod A3-6-4 of the HBEP3 (High Burnup Effects Programme Final Report, 2002) experiment and simulations with the fitting formulae included in DIONISIO.

and then decreases (Spino et al., 2006). This fact reveals that after ≈100 MWd/kgU the pores coalescence process becomes significant. In the burnup range beyond the critical value, the pore density decreases while larger pores are generated as the burnup increases.

For these reasons, two different schemes have been adopted to represent the system state in terms of the local burnup level: *model 1*, valid for burnups between 60 and 100 MWd/kgU and *model 2*, for burnups above 100 MWd/kgU. (For local burnup values even higher, the pores next to the pellet surface are postulated to acquire an increasing probability of making contact with the free surface and thus becoming open pores). The microstructure adopts a typical aspect referred to as *ultra high burnup structure* (UHBS). The experimental data reveal that the fraction of open pores remains low and limited to a very narrow layer in the pellet periphery. Spino et al. (1996) determined that a local burnup as high as 250 MWd/kgU is necessary for reaching a total porosity of 24%. Below this burnup level, the open porosity represents less than 7% of the total porosity. These very high local burnup levels should be necessary in order that the pores made contact with the pellet surface thus releasing its gas content. The model predicts that the fraction of open pores decreases towards the pellet interior so that the vented zone should be limited to the outer 20 μm layer. The complete model is described elsewhere (Martín Lemes et al., 2014; Estudio analítico y numérico de los efectos de la irradiación hasta alto quemado en combustibles de reactores de potencia, 2013). Only the more relevant aspects will be explained here.

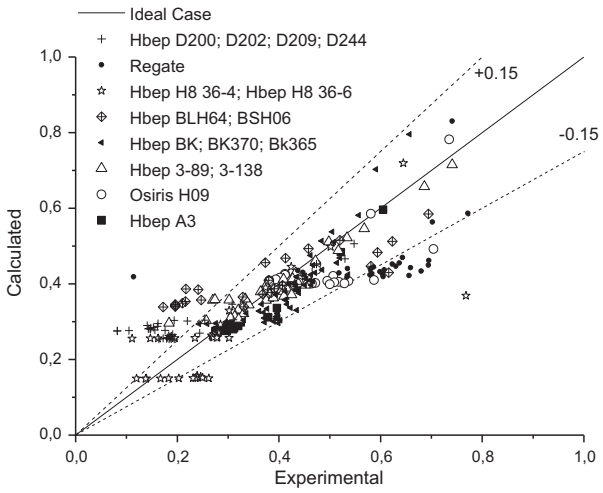

Fig. 10. Comparison between experimental measures of Cesium vs. Calculated by DIONISIO code in HBEP (High Burnup Effects Programme Final Report, 2002), OSIRIS(Rapport d'Assurance Qualite Crayon FF06E2BV/G07/1067, 1998) and REGATE(NEA, 2004) experiments.

- Pores are assumed of spherical shape with radius R_p. The pores population within the material is characterized by the porosity (σ) and pores density (n_p), which are related by $\sigma = \frac{4}{3}\pi R_p^3 n_p$.
- The accumulation of fission gas within the closed pores gives rise to a certain overpressure on the pore surface given by $\Delta\zeta = P_p - \frac{2\gamma}{R_p} - P_h$where P_p is the pressure due to the gas within the pore, P_h is the hydrostatic pressure and γ is the surface energy of the pore, estimated in $\gamma \approx 1 J/m^2$.

Author's personal copy

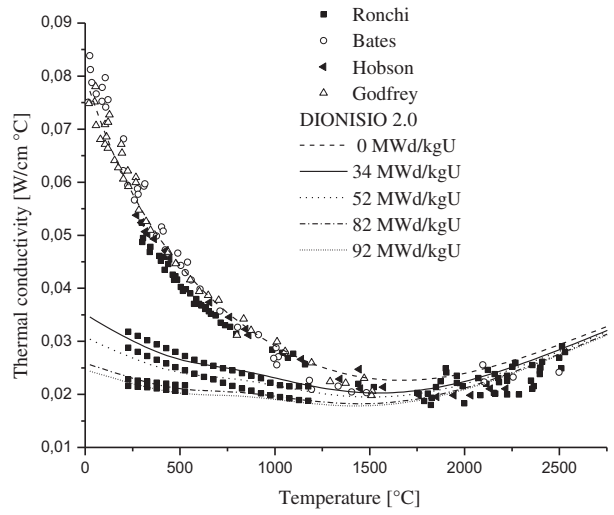

Fig. 11. Effect of burnup on the thermal conductivity of UO_2.

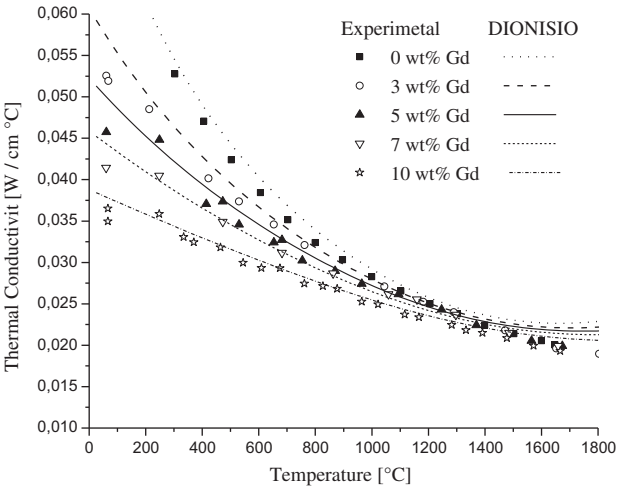

Fig. 12. Effect of Gd content on thermal conductivity of UO_2.

- The gas enclosed in the pores, mainly Xe, is assumed to obey the Van der Waals equation. Then, $P_p(\frac{4}{3}\pi R_p^3 - \omega_{Xe}N_p) = N_p kT$ where $\omega_{Xe} \approx 8.5 \times 10^{-29}$ m^3/atom, is the specific volume for *Xe*, N_p is the number of gas atoms in a pore and T is the absolute temperature. The number of fission gas atoms enclosed in the pores per unit volume of the material is $C_p = N_p n_p$ and then $P_p(\sigma - \omega_{Xe}C_p) = C_p kT$.
- The fission gas generated during fuel irradiation, c_{gen}, is distributed among pores, c_p, matrix, c_{matrix}, and rod free volume, c_{rel}, i.e.: $c_{gen} = c_p + c_{matrix} + c_{rel}$, all of them measured as weight percent of fuel.
- In the burnup range corresponding to *model one* c_{rel} is very low and can be approximated by $c_{rel} \approx 1.6 \times 10^{-6}$ wt%. The empirical expression $\sigma = \left[\frac{(0.015+0.008\lambda)Bu}{1-0.0135\times Bu+6\times 10^{-5}Bu^2}\right] - (0.036 - \sigma_0)$ was developed for porosity in terms of local burnup. It includes the possible effects of pellet-cladding mechanical interaction ($\lambda = 1$ when pellet-cladding contact exists and $\lambda = 0$ when it does not). σ_0 represents the porosity reached by the fuel material when Bu = Bu$_o$ = 60 MWd/kgU, i.e. when the high burnup range starts. The value of σ_0 is usually in the range 3–6%, depending on the fabrication route and base irradiation conditions.

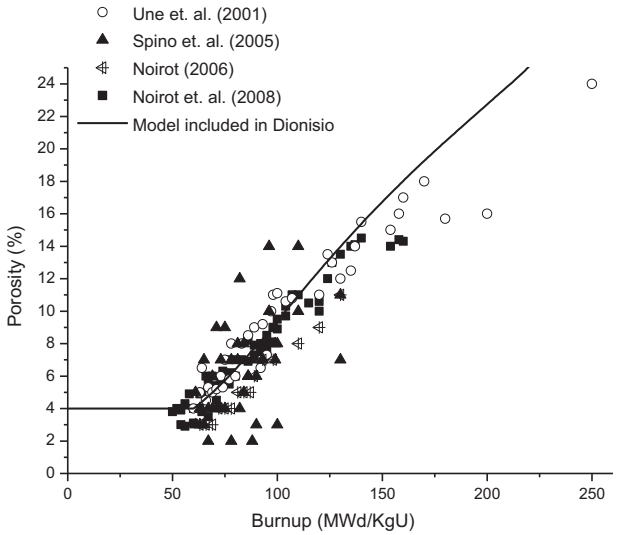

Fig. 13. Porosity vs. burnup. Comparison between experimental data and the model developed for DIONISIO.

- *Model two* includes the mechanisms of pore growth due to trapping of vacancies and interstitials, and to interactions of diverse orders between pores (closed or open) and of pores with the pellet surface. According to (Blair, 2008; Olander, 1976; Khvostov et al., 2011) the pore radius growth rate is given by $\frac{dR_p}{dt} = \frac{1}{R_p}[D_v X_v^0(1 - \exp(-\frac{\Delta\zeta\Omega}{kT})) - D_i X_i^0(1 - \exp(\frac{\Delta\zeta\Omega}{kT}))]$ where Ω indicates the volume associated to the point defects assumed equal to the volume per uranium atom in the UO_2 lattice ($\Omega = 4.09 \times 10^{-29}$ m^3), the term $\Delta\zeta\Omega$ in both exponents represents the work invested in moving an atom under a pressure $\Delta\zeta$ thus creating a point defect of volume Ω; $X_{v,i} = \Omega C_{v,i}$ indicates the fraction of sites occupied by vacancies/interstitials. A system of coupled differential equations is solved to obtain the fractional concentrations of vacancies and interstitials, which lead to the pore radius R_p.

The complete model is compared with experimental data obtained from the open literature (Noirot et al., 2008; Une et al., 2001; Spino et al., 2005; Noirot, 2006). The results are shown in Fig. 13.

6. Conclusions

Several subroutines have been incorporated to the DIONISIO code in recent times. They are oriented to extending the scope of the code to the high burnup range. The radial profiles of the more significant Uranium and Plutonium isotopes are evaluated, assuming that the resonant absorption of epithermal neutrons by ^{238}U is responsible for the formation of the rim structure. The degradation of thermal conductivity with burnup as well as its dependence with the content of gadolinium, usually included as burnable poison, were also considered. Empirical models describing the production of *Nd*, *Cs* and *Xe* were incorporated to the code.

A more complex model aimed at describing the formation and progress of the high burnup microstructure was also incorporated. The evolution of parameters like porosity and pore number density of closed and open pores, overpressure provoked by the fission gas enclosed in the pores, concentration of point defects in the vicinity of these pores, inventory of gas retained in the solid matrix of the transformed pellet region, trapped in the pores and released to the rod free volume are considered in terms of the burnup, in the range between 60 and 300 MWd/kgU, as well as in terms of the radial position within the fuel pellet in its outer ring.

Author's personal copy

All the subroutines were subjected to numerous separate tests that included parametric analyses spanning a wide range of temperature, burnup, fission rate, surface/volume ratio, among others. The model testing also covered comparison of its results with experimental information mostly obtained from the FUMEX I/II/III data bank showing a good agreement both in the average burnup as well as in the total plutonium produced.

With the improvements recently introduced, involving subroutines for the physical and chemical properties of the fuel material in the high burnup range, the code DIONISIO in its version 2.0 evidenced a good performance in the numerous simulations of experimental situations typical of PWR, BWR and PHWR fuels. On this basis, DIONISIO 2.0 can be regarded as an adequate simulation tool even for average burnup levels as high as 60 MWd/kgU.

References

Blair, P., 2008. PhD Thesis, Modelling of fission gas behaviour in high burnup nuclear fuel, École Polytechnique Federale, Lausanne, Suiza.

C. Grant – User Handbook of the HUEMUL Code, 2014.

Denis, A., Soba, A., 2003. Simulation of pellet-cladding thermomechanical interaction and fission gas release. Nucl. Eng. Des. 223.

Eduardo Villarino CONDOR CALCULATION PACKAGE PHYSOR, 2002. Korea.

Estudio analítico y numérico de los efectos de la irradiación hasta alto quemado en combustibles de reactores de potencia, 2013. Master Thesis, Martín Lemes.

Fink, J., 2000. Review: thermophysical properties of uranium dioxide. J. Nucl. Mater. 279.

González, M., Denis, A., Soba, A., Modelización de la conductividad térmica del UO_2 y $(U, Gd)O_2$ bajo irradiación. Implementación en el código DIONISIO, 98° Reunión Anual de la Asociación Física Argentina, 24–27 de septiembre de 2013, Bariloche, Argentina.

HELIOS Methods, 1998. Program Manual Rev. 1, Program HELIOS 1.4, Studsvik-Scandpower.

NEA-1510 IFPE/HBEP-3 REV.1 – High Burnup Effects Programme Final Report, DOE/NE/34046-1 [HBEP-61(3P27)], 2002.

<http://www.iaea.org>, 2014.

<http://www.oecd-nea.org/science/fuel/ifpelst.html>, 2014.

Hutton, J.L., Newton, T.D., Perry, R.J., Powney, D.J., 2004. In: Proceedings of PHYSOR 2004 – The Physics of Fuel Cycles and Advanced Nuclear Systems: Global Developments, Session 1D, American Nuclear Society, Chicago, Illinois, USA.

IAEA-TECDOC-1687, 2012. Fuel Modelling at Extended Burnup (FUMEX-II), IAEA.

IFPE/RISOEIII, NEA-1493/17, 1995.

Khvostov, G., Mikityuk, K., Zimmermann, M., 2011. A model for fission gas release and gaseous swelling for the uranium dioxide fuel coupled with the FALCON code. Nucl. Eng. Des. 241.

Killeen, J., Sartori, E., Tverberg, T., 2009. FUMEX-III: a new IAEA coordinated research project on fuel modelling at extended burnup. Top Fuel.

Kinoshita, M., 1997. Towards the mathematical modeling of rim structure formation. J. Nucl. Mater. 248.

Lassmann, K., Walker, C.T., van de Laar, J., Lindström, F., 1995. Modeling the high burnup UO_2 structure in LWR fuel. J. Nucl. Mater. 226, 1–8.

Lassmann, K., Schubert, A., Van De Laar, J., 2003. Recent developments of the transuranus code with emphasis on high burnup phenomena. In: International Conference on Nuclear Fuel for Today and Tomorrow.

Lee, Chan Bock, Kim, Dae Ho, Song, Jae Seung, Bang, Je Gun, Jung, Youn Ho, 2000. RAPID model to predict radial burnup distribution in LWR UO_2 fuel. J. Nucl. Mater. 282.

Martín Lemes, Alejandro Soba, Alicia Denis AN EMPIRICAL FORMULATION TO DESCRIBE THE EVOLUTION OF THE HIGH BURNUP STRUCTURE, (Under evaluation), 2014.

Massih, A.R., Persson, S., Weiss, Z., 1992. Modelling of $(U,Gd)O_2$ fuel behaviour in boiling water reactors. J. Nucl. Mater. 188.

NEA-1696 IFPE/REGATE L10.3, 2004.

Newton, T.D., Hutton, J.L., 2002. In: Park, M.G., (Ed.), Proceedings of PHYSOR 2002 – International Conference on the New Frontiers of Nuclear Technology: Reactor Physics, Safety and High-Performance Computing, 14A-04, American Nuclear Society, Seoul, Korea.

Noirot, L., 2006. An advanced mechanistic model of fission gas behavior in nuclear fuel. J. Nucl. Sci. Technol. 43.

Noirot, J., Desgranges, L., Lamontagne, J., 2008. Detailed characterisations of high burn-up structures in oxide fuels. Nucl. J. Mater. 372.

Olander, D., 1976. Fundamental Aspects of Nuclear Reactor Fuel Elements. Department of Nuclear Engineering, University of California, Berkeley.

Rapport d'Assurance Qualite Crayon FF06E2BV/G07/1067, 1998.

Rapport d'Assurance Qualite Crayon FF0EFELX/H09/5007, 1998.

Ronchi, C., Scheindlin, M., Staicu, D., Kinoshita, M., 2004. Effect of burn-up on the thermal conductivity of uranium dioxide up to 100,000 MWd/t. J. Nucl. Mater. 327.

Schubert, A., Van Uffelen, P., van de Laar, J., Walker, C.T., Haeck, W., 2008. Extension of the TRANSURANUS burn-up model. J. Nucl. Mater. 376.

Simulación del comportamiento termomecánico de una barra combustible en operación, 2007. Alejandro Soba. Tesis de doctorado, FCEyN, UBA

Soba, A., Denis, A., 2008. Simulation with Dionisio 1.0 of thermal and mechanical pellet-cladding interaction in nuclear fuel rods. J. Nucl. Mater. 374.

Soba, A, Denis, A., Romero, L., Villarino, E., Sardella, F., 2013. A high burnup model developed for the DIONISIO code. J. Nucl. Mater. 433.

Spino, J., Vennix, K., Coquerelle, M., 1996. Detailed characterization of the rim microstructure in PWR fuels in the burn-up range 40–67 GWd/tM. J. Nucl. Mater. 231.

Spino, J., Rest, J., Goll, W., Walker, C.T., 2005. Matrix swelling rate and cavity volume balance of UO_2 fuels at high burn-up. J. Nucl. Mater. 346.

Spino, J., Stalios, A.D., Santa Cruz, H., Baron, D., 2006. Stereological evolution of the rim structure in PWR-fuels at prolonged irradiation: dependencies with burn-up and temperature. J. Nucl. Mater. 354.

Stammler, R.J.J., Boerresen, S., Casal, J.J., Forslund, P., 1996. In: Proceedings of PHYSOR 1996 – International Conference on Physics of Reactors, American Nuclear Society, Japan.

Une, K., Nogita, K., Shiratori, T., Hayashi, K., 2001. Rim structure formation of isothermally irradiated UO_2 fuel discs. J. Nucl. Mater. 288.